geosciences

MDPI

Correction

Correction: Bernardi et al. OH-Defects in Detrital Quartz Grains from the Julian Basin (NE Italy and Slovenia): A Fourier Transform Infrared Study. *Geosciences* 2022, *12*, 90

Francesco Bernardi [1,*], Henrik Skogby [2] and Davide Lenaz [1]

[1] Department of Mathematics and Geosciences, University of Trieste, 34128 Trieste, Italy; lenaz@units.it
[2] Department of Geosciences, Swedish Museum of Natural History, SE-10405 Stockholm, Sweden; henrik.skogby@nrm.se
* Correspondence: francesco.bernardi@phd.units.it

The authors would like to correct the published article [1].

There was an error in the original publication. Due to a calculation mistake, water contents had been estimated at half of the real values. The corrections are mere substitutions of the wrong values with the corrected ones in the text and table; slight changes have also been made in the subdivisions and groupings in figures and the text.

Corrections have been made to Figures 4 and 5, Table A1, and paragraphs in Sections 3.2.1, 3.2.2 and 4. The corrected paragraphs are as follows:

3.2.1. Al-Related Defects

The Al-related substitution appears as a triplet peak at wavenumbers 3310–3378–3430 cm^{-1} (Figure 3). Within the samples analyzed, it shows a great variation in water content, from 0.8 ppm (JB26) to 214 ppm (JB17) (Table A1 in Appendix A). Quartz crystals in JB1 show a moderate variety with four grains in the range 0–5 ppm, three grains between 5 and 10 ppm, four grains in the range 10–15 ppm, one between 15 and 20 ppm, and two between 20 and 50 ppm. Samples in JB23 and JB26 show similar content of Al defects (0.8–13 ppm). In JB23, 12 quartz crystals show water content lower than 5 ppm, and four between 5 and 10 ppm; while in JB26, there are three grains over the threshold of 5 ppm: two in the 5–10 ppm range and one between 10 and 15 ppm.

A clearly different behavior is revealed for sample JB17, with 10 grains under 10 ppm, one between 10 ppm and 15 ppm, and four even over 50 ppm (80 ppm, 112 ppm, 140 ppm, and 214 ppm) (Figure 4).

3.2.2. Li-Related Defects

The Li-related substitution appears as a single peak at a wavenumber of 3480 cm^{-1} (Figure 3). Compared with Al defects, the Li-related substitutions are less abundant but still present similar patterns. Samples JB23 shows one grain with less than 0.5 ppm, and one between 0.5 and 1 ppm; the only grain from JB26 has a value under 0.5 ppm. Sample JB17 presents the greatest number of substitutions and also the greatest variety, with three grains over 5 ppm (8.4 - 9.8 - 15 ppm). As for Al-related defects, JB23 and JB26 show very similar properties, whereas JB1 presents a relevant difference from JB23 and JB26 in terms of values. JB17 shows again a distinctly different behavior with more grains with this defect and higher water contents.

Citation: Bernardi, F.; Skogby, H.; Lenaz, D. Correction: Bernardi et al. OH-Defects in Detrital Quartz Grains from the Julian Basin (NE Italy and Slovenia): A Fourier Transform Infrared Study. *Geosciences* 2022, *12*, 90. *Geosciences* **2023**, *13*, 127. https://doi.org/10.3390/geosciences13050127

Received: 16 March 2023
Accepted: 17 April 2023
Published: 25 April 2023

Copyright: © 2023 by the authors. Licensee MDPI, Basel, Switzerland. This article is an open access article distributed under the terms and conditions of the Creative Commons Attribution (CC BY) license (https://creativecommons.org/licenses/by/4.0/).

4. Discussion

In this study, a total of 80 crystals were analyzed from four Julian Basin samples. The frequency of crystals displaying each defect is shown for comparison in Figure 2e. The total amount of OH is in the range 0–30 ppm for JB1, 0–224 ppm for JB17, 0–9.0 ppm for JB23, and 0–13 ppm for JB26.

Sample JB1 is the oldest in the stratigraphic column (ca. 66 Ma). The grains from this sample show moderate variability in defects, with an abundance of single Al-related defects and only a few of the other types. The water content for Al defects spans from 2.4 to 30 ppm. Other defects are present in only one grain each, with the water contents of Li: 2.6 ppm, 4H: 2.6 ppm, and B: 0.6 ppm. The observations suggest that both metamorphic and non-metamorphic sources are present [18,27].

Samples JB23 and JB26 are the youngest in the stratigraphic column and are almost coeval (between 52 and 53 Ma). These two samples display very similar behaviors, with a great number of grains bearing Al defects but corresponding to low water contents, for JB23, between 0.8 and 8.8 ppm, and for JB26, between 0.8 and 13 ppm. Li-related substitutions are in the range of 0.2–0.6 ppm, in grains from JB23, and 0.2 ppm in the only grain in JB26. There are no B-related substitutions. An almost solely metamorphic origin can be suggested for these samples, according to the above-mentioned correlations [18,27].

Sample JB17 is slightly older than JB23 and JB2, but considerably younger than JB1, with an age of about 56 Ma. The spectra of the grains from this sample show different patterns to those of the others, both in terms of defect variability and the corresponding water contents. In this sample, almost half of the grains show defects with multiple substitutions (Al + Li, Al + B, Al + 4H, and Al + Li + B) (Figure 2e), with very high values of water content, especially for the Al-related defect (1.6–214 ppm, Figure 4). The Li-related defect shows high variability and the highest content within the basin (1.8–15 ppm), and the same is observed for B (0.1–0.6 ppm), which also shows the highest values. The 4H defect shows no great variability and average content (0.2–1.0 ppm). The great number of Al- and Li-related defects, and their notable variability, suggests the presence of a mainly volcanic source, possibly even late-stage volcanic (hydrothermal Li defect [20]) source material. The presence of 4H defects indicates that there is also a supply from high-pressure rocks.

In order to determine the source rocks of the detrital quartz, we need to consider the previous studies on the Julian Basin.

Cr-spinel chemistry indicates they were derived from the Dinarides [13,16]. Based on the Fe^{2+}/Fe^{3+} and TiO_2 content of Cr spinels, it is possible to discriminate between peridotitic (or restitic spinels) and magmatic (crystallized from percolating melts within the peridotites) [13,35]. These parameters show that, for samples JB1, JB23, and JB26, more than 60% of the Cr-spinels are peridotitic, while in JB16 (stratigraphically close to JB17 studied here), they represent only 40% of the Cr spinels (Figure 2c).

Within the peridotitic spinels, there is a widespread distribution for JB1 and JB17, while they are concentrated within the 50–70 Cr# interval for the two Eocene samples (JB23 and JB26). The magmatic spinels show a clear shift to low Cr# values (<40) in JB17 and JB23 samples. The chemistry of the volcanic spinels demonstrates that at least four different source areas were present in the area including (1) MORB or MORB-type back-arc rocks that are mainly present in JB16, (2) subduction-related back-arc and continental rifting, (3) plume-related intraplate basalts, and (4) island arc tholeiites or boninites [13,16].

The main spinel detritus in the Julian Basin derived from the suprasubduction zone of the Vardar Ocean during the beginning of deposition in the Maastrichtian [36]. These supplies continued during the Paleocene, when MORB-type spinels from the spreading ridge of the Pindos Ocean arrived as well. Successively, a new input of suprasubduction zone detritus arrived during the Early Eocene times, possibly related to the intra-oceanic subduction of the Pindos Ocean. It is interesting to note that the Vardar and Pindos areas are divided by the Drina–Ivanica microcontinent.

Recently, trace and rare earth (RE) elements in garnets have been studied from the region [14]. The authors analyzed about 250 garnets from different basins in the SE Alps,

including in the Julian Basin, where the most common types are, according to Mange and Morton [37] classification, Bi, Bii, and Ci, with very low amounts of A and D. Almost 90% of garnets from JB1 belong to the Bii and Ci types, almost 85% of garnets from JB23 are in the B typology, JB26 shows a wider spread distribution (including D type), while JB17 present contributions that are equally distributed between the Bi, Bii, and Ci types (Figure 2d). Even if the authors did not link the supplies to specific sources, it is possible to suppose that the Ci-type garnets were supplied from the suprasubduction zone (SSZ) of the Vardar ophiolites and their metamorphic soles. The presence of garnets related to granitoids and metasediments (B-type garnets are related to amphibolite facies metasediments [37]) possibly involves contributions from different ophiolitic sources but also from the Drina–Ivanica terrane. Upper Jurassic granitoid rocks associated with the East Vardar ophiolites form a discontinuous belt from Serbia in the north to northern Greece in the south. Two groups of intraophiolitic granitoids are distinguished: (1) diorite, quartz diorite, and quartz monzodiorite; and (2) two subgroups of granites and granodiorites [38]. However, none of these granitoids is garnet-bearing.

Detrital amphiboles (actinolite, Mg-hornblende, barroisite, and glaucophane) associated with pyroxenes have been found in Lower Eocene (about 52 Ma) turbidites of the Julian Basin [15]. These samples are stratigraphically located between JB23 and JB26. Actinolite and Mg-hornblende are derived from low-to-medium-grade metamorphic rocks (metavolcanics in greenschist facies). Barroisite is the ultra-high-pressure type of calcic amphibole, and it is considered a marker of retrogressive metamorphism. Glaucophane is representative of high-pressure blueschist facies metamorphic rocks. Omphacites are related to subsolidus recrystallization of basic igneous rocks at high-pressure and temperature in eclogite facies. The occurrences of these minerals are commonly related to the erosion of high-pressure-low-temperature metavolcanics in green-blue schist and eclogitic facies. According to the low amount and distribution of these minerals, it has been suggested that they belong to limited metamorphic bodies exhumed at about 56 Ma during a phase of uplift of the Dinarides [15,39].

As regards the geochemistry of the basinal sediments, the oceanic source of sediments at 56 Ma (sample JB16) is confirmed by De Min et al. [17]. There are different parameters that can be used to prove the source of the sediments. The Cr/V ratio reveals that sample JB16 (Cr/V = 33.22) has a non-peridotitic source (that spans between 2 and 20). Additionally, the study of trace and RE elements can provide further information about the source of the sediments. Variations in chemical ratios within the stratigraphic column of Julian Basin display this difference. In fact, considering Zr/Y and $(La/Sm)_{UCn}$, it is clear that the greater variation corresponds to sample JB16. This variation seems to demonstrate the paroxysmal moment of the Dinaric orogenesis [17] (Figure 2b).

The present study shows that the detrital quartz crystals in the Julian Basin show different patterns of defects and different water contents, suggesting differences in sediment source. There is a change from the bottom of the stratigraphic sequence, where a mixed igneous and non-igneous source is present, and the top, where an almost solely metamorphic rock-type source occurs. As observed for other mineral systematics, quartz from sample JB17 show the greatest variability in supplies. The abundance and heterogeneity in the types of defects, the water content (up to over 200 ppm for Al related, and from 1.8 to 15 ppm for Li related), and their great variability suggest a more complex source for the sediments, with the magmatic component dominant over the metamorphic component. These features confirm the distinctive provenance in this part of the sequence, in line with previous studies (Figure 5).

According to the previous interpretations [13,14,36], it is possible that the main volcanic detrital quartz could be supplied from the Drina–Ivanica microcontinent or the intraophiolitic Jurassic granitoids, while the metamorphic quartz is related to the metamorphic soles of ophiolitic emplacement related to the closure of the Vardar (JB1 and JB17) and Pindos oceans (JB23 and JB26), respectively.

New studies are currently ongoing with more samples, in order to verify if there was a paroxysmal event at about 56 Ma (JB17), or if the change in quartz supplies starts between the beginning of deposition at 67 Ma (JB1) and JB17. Chemical analyses on the same grains will add more constraints to the genesis of the quartz crystals. The most common trace elements in magmatic quartz are Al, Li, and Ti, with medians of 447, 39.6, and 17.4 ppm in S-type rare-metal granites, and 160, 15, and 6.6 ppm in A-type rare-metal granites [40]. It is possible that the coupling of OH-defect data with the trace element content of quartz will better discriminate granitoid sources.

The updated Figure 4 is:

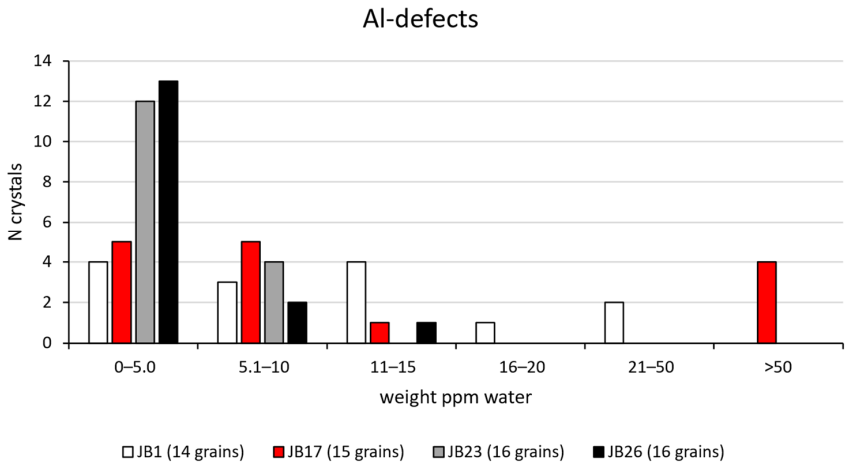

Figure 4. Quantification of the Al-related OH-defects calculated with calibration by Thomas et al. [34]. Samples without recognizable peaks are omitted.

The updated Figure 5 is:

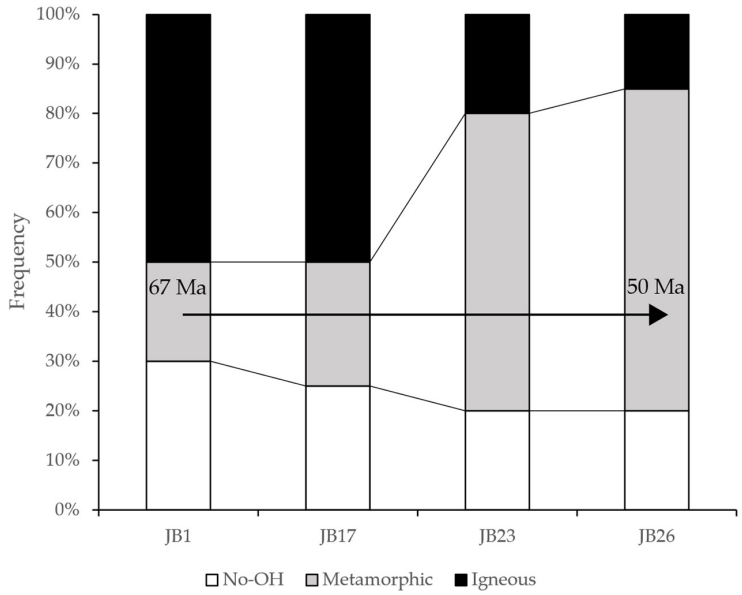

Figure 5. Frequencies of quartz grains from igneous and non-igneous sources from 67 to 50 Ma. As igneous quartz, we considered all grains with OH > 5 ppm according to [18,19].

The updated Table A1 is:

Table A1. Water content for samples calculated with Thomas et al. [34] (shaded column) and Libowitzky and Rossman [25] calibrations. ND means that no recognizable spectra were detected.

Sample	Thickness	Wavenumber	Absorption Integration	Density	ε	H_2O ppm [34]	ε	H_2O ppm [25]	Defect
JB1_001	215	3375	1.44	2.65	89,000	10	93,220	9.8	Al
JB1_002	230	ND	ND	2.65	89,000	ND	ND	ND	-
JB1_003	260	ND	ND	2.65	89,000	ND	ND	ND	-
JB1_004	276	ND	ND	2.65	89,000	ND	ND	ND	-
JB1_005	144	3585	0.25	2.65	89,000	2.6	41,430	5.7	4H+
JB1_006	171	3370	0.56	2.65	89,000	5.0	94,450	4.7	Al
JB1_007	147	3371	2.81	2.65	89,000	29	94,200	28	Al
JB1_008	175	3368	0.49	2.65	89,000	4.3	94,940	4.0	Al
JB1_009	181	3369	1.34	2.65	89,000	11	94,690	11	Al
JB1_010	146	ND	ND	2.65	89,000	ND	ND	ND	-
JB1_011	254	3380	0.41	2.65	89,000	2.5	91,980	2.4	Al
JB1_012	73	3379	0.60	2.65	89,000	13	92,230	12	Al
JB1_013	179	ND	ND	2.65	89,000	ND	ND	ND	-
JB1_014	153	3374	1.66	2.65	89,000	17	93,460	16	Al
JB1_015	63	3370	0.52	2.65	89,000	13	94,450	12	Al
JB1_016	128	3368	1.89	2.65	89,000	23	94,940	21	Al
		3480	0.21	2.65	89,000	2.5	67,320	3.3	Li
JB1_017	187	3365	0.83	2.65	89,000	6.8	95,680	6.3	Al
JB1_018	158	3364	0.59	2.65	89,000	5.7	95,930	5.3	Al
JB1_019	280	3378	0.52	2.65	89,000	2.8	92,480	2.7	Al
		3595	0.09	2.65	89,000	0.5	38,960	1.1	B
JB1_020	218	3380	0.73	2.65	89,000	5.1	91,980	5.0	Al
JB17_001	251	3379	1.09	2.65	89,000	6.6	92,230	6.4	Al
JB17_002	189	ND	ND	2.65	89,000	ND	ND	ND	-
JB17_003	107	3371	0.21	2.65	89,000	3.0	94,200	0.3	Al
		3585	0.01	2.65	89,000	0.1	41,430	0.3	4H+
JB17_004	162	3367	22.75	2.65	89,000	214	95,190	200	Al
		3480	1.04	2.65	89,000	9.8	67,320	13	Li
JB17_005	180	3370	0.75	2.65	89,000	6.4	94,450	6.0	Al
JB17_006	104	ND	ND	2.65	89,000	ND	ND	ND	-
JB17_007	165	3376	1.46	2.65	89,000	14	92,970	13	Al
		3480	0.2	2.65	89,000	1.9	67,320	2.5	Li
JB17_008	197	3372	0.23	2.65	89,000	1.8	93,960	1.7	Al
JB17_009	237	3371	0.25	2.65	89,000	1.6	94,200	1.5	Al
JB17_010	149	ND	ND	2.65	89,000	ND	ND	ND	-
JB17_011	224	3368	0.33	2.65	89,000	2.3	94,940	2.1	Al
		3595	0.02	2.65	89,000	0.1	38,960	0.3	B
JB17_012	110	3377	0.57	2.65	89,000	7.9	92,720	7.6	Al
JB17_013	200	ND	ND	2.65	89,000	ND	ND	ND	-
JB17_014	207	3365	0.23	2.65	89,000	1.7	95,680	1.6	Al
JB17_015	221	3378	1.49	2.65	89,000	10	92,480	9.9	Al
JB17_016	144	3371	10.55	2.65	89,000	112	94,200	106	Al
		3585	0.09	2.65	89,000	1.0	41,430	2.1	4H+
JB17_017	162	3363	14.91	2.65	89,000	140	96,170	130	Al
		3480	1.58	2.65	89,000	15	67,320	20	Li
		3595	0.06	2.65	89,000	0.6	38,960	1.3	B
JB17_018	171	ND	ND	2.65	89,000	ND	ND	ND	-
JB17_019	233	3369	12.05	2.65	89,000	79	94,690	74	Al
		3480	1.27	2.65	89,000	8.3	67,320	11	Li
		3595	0.08	2.65	89,000	0.5	38,960	1.2	B
JB17_020	177	3370	0.74	2.65	89,000	6.4	94,450	6.0	Al

Table A1. *Cont.*

Sample	Thickness	Wavenumber	Absorption Integration	Density	ε	H_2O ppm [34]	ε	H_2O ppm [25]	Defect
JB23_001	283	3373	0.21	2.65	89,000	1.1	93,700	1.1	Al
JB23_002	129	3362	0.3	2.65	89,000	3.6	96,420	3.3	Al
JB23_003	206	3373	0.32	2.65	89,000	2.4	93,710	2.3	Al
JB23_004	251	3371	0.27	2.65	89,000	1.6	94,200	1.6	Al
JB23_005	242	ND	ND	2.65	89,000	ND	ND	ND	-
JB23_006	199	ND	ND	2.65	89,000	ND	ND	ND	-
JB23_007	279	3372	0.39	2.65	89,000	2.1	93,960	2.0	Al
JB23_008	238	3364	0.53	2.65	89,000	3.4	95,930	3.2	Al
		3585	0.14	2.65	89,000	0.9	41,430	1.9	4H+
JB23_009	186	3367	0.79	2.65	89,000	6.5	95,190	6.1	Al
JB23_010	245	3365	0.14	2.65	89,000	0.9	95,680	0.8	Al
JB23_011	215	3368	0.15	2.65	89,000	1.1	94,940	1.0	Al
JB23_012	167	3373	0.78	2.65	89,000	7.1	93,710	6.8	Al
JB23_013	93	ND	ND	2.65	89,000	ND	ND	ND	-
JB23_014	179	3369	0.34	2.65	89,000	2.9	94,690	2.7	Al
JB23_015	197	3375	0.3	2.65	89,000	2.3	93,220	2.2	Al
JB23_016	167	3367	0.41	2.65	89,000	3.8	95,190	3.5	Al
		3480	0.07	2.65	89,000	0.6	67,320	0.9	Li
JB23_017	206	3374	0.14	2.65	89,000	1.0	93,460	1.0	Al
JB23_018	162	3373	0.71	2.65	89,000	6.7	93,710	6.4	Al
JB23_019	191	3375	1.09	2.65	89,000	8.7	93,220	8.3	Al
		3480	0.03	2.65	89,000	0.2	67,320	0.3	Li
JB23_020	202	ND	ND	2.65	89,000	ND	ND	ND	-
JB26_001	209	3375	0.11	2.65	89,000	0.8	93,220	0.8	Al
JB26_002	211	3372	0.94	2.65	89,000	6.8	93,960	6.4	Al
		3480	0.02	2.65	89,000	0.1	67,320	0.2	Li
JB26_003	197	3372	0.36	2.65	89,000	2.8	93,960	2.6	Al
JB26_004	186	3377	1.63	2.65	89,000	13	92,720	13	Al
JB26_005	287	3367	0.3	2.65	89,000	1.6	95,190	1.5	Al
JB26_006	233	ND	ND	2.65	89,000	ND	ND	ND	-
JB26_007	270	3369	0.47	2.65	89,000	2.7	94,690	2.5	Al
JB26_008	223	ND	ND	2.65	89,000	ND	ND	ND	-
JB26_009	186	ND	ND	2.65	89,000	ND	ND	ND	-
JB26_010	256	ND	ND	2.65	89,000	ND	ND	ND	-
JB26_011	252	3376	0.34	2.65	89,000	2.1	92,970	2.0	Al
JB26_012	242	3366	0.24	2.65	89,000	1.5	95,430	1.4	Al
JB26_013	104	3362	0.29	2.65	89,000	4.3	96,420	4.0	Al
JB26_014	181	3374	0.15	2.65	89,000	1.3	93,460	1.2	Al
JB26_015	218	3374	0.31	2.65	89,000	2.2	93,460	2.1	Al
JB26_016	270	3374	1.41	2.65	89,000	8.0	93,460	7.6	Al
JB26_017	235	3367	0.36	2.65	89,000	2.3	95,190	2.2	Al
JB26_018	90	3374	0.16	2.65	89,000	2.7	93,460	2.6	Al
JB26_019	140	3362	0.24	2.65	89,000	2.6	96,420	2.4	Al
JB26_020	163	3370	0.39	2.65	89,000	3.7	94,450	3.4	Al
		3585	0.02	2.65	89,000	0.2	41,430	0.4	4H+

The authors apologize for any inconvenience this has caused for the readers. The authors state that the scientific conclusions are unaffected. This correction was approved by the Academic Editor. The original publication has also been updated.

Reference

1. Bernardi, F.; Skogby, H.; Lenaz, D. OH-Defects in Detrital Quartz Grains from the Julian Basin (NE Italy and Slovenia): A Fourier Transform Infrared Study. *Geosciences* **2022**, *12*, 90. [CrossRef]

Disclaimer/Publisher's Note: The statements, opinions and data contained in all publications are solely those of the individual author(s) and contributor(s) and not of MDPI and/or the editor(s). MDPI and/or the editor(s) disclaim responsibility for any injury to people or property resulting from any ideas, methods, instructions or products referred to in the content.